# MesoTIRF: a novel axial super-resolution illuminator for membrane imaging over a 4.4 mm x 3.0 mm field of view

Shannan Foylan, William Amos, John Dempster, Lisa Kölln, Carsten Hansen, et al.

Shannan Foylan, William B. Amos, John Dempster, Lisa Kölln, Carsten G. Hansen, Michael Shaw, Gail McConnell, "MesoTIRF: a novel axial super-resolution illuminator for membrane imaging over a 4.4 mm x 3.0 mm field of view," Proc. SPIE 12386, Single Molecule Spectroscopy and Superresolution Imaging XVI, 1238604 (15 March 2023); doi: 10.1117/12.2649070

SPIE.

Event: SPIE BiOS, 2023, San Francisco, California, United States

# MesoTIRF: a novel axial super-resolution illuminator for membrane imaging over a 4.4 mm x 3.0 mm field of view

**Shannan Foylan** [a, *], William B. Amos [b], John Dempster [b], Lisa Kölln [a, c, d], Carsten G. Hansen [c, d], Michael Shaw [e, f] and Gail McConnell [b]

[a] Department of Physics, University of Strathclyde, Glasgow G4 0NG, UK
[b] Strathclyde Institute for Pharmacy & Biomedical Sciences, University of Strathclyde, Glasgow, G4 0RE, UK
[c] Centre for Inflammation Research, University of Edinburgh, Edinburgh, EH16 4TJ, UK
[d] Institute for Regeneration and Repair, University of Edinburgh, Edinburgh, EH16 4UU, UK
[e] Department of Chemical and Biological Sciences, National Physical Laboratory, Teddington, TW11 0LW, UK
[f] Department of Computer Science, University College London, London, WC1E 6BT, UK

*shannan.foylan@strath.ac.uk

## ABSTRACT

In Total Internal Reflection Fluorescence (TIRF) microscopy, a specimen is illuminated by the evanescent field produced by a beam undergoing total internal reflection, whose characteristic depth is orders of magnitude below the axial diffraction limit. The axial super-resolution and much improved contrast of TIRF gives a substantially improved signal-to-background ratio (SBR) than that which can be achieved with widefield illumination, and it is used extensively for imaging of the cell membrane [1]– [3] .

Commercial TIRF objectives allow for a simple adaption to existing microscope systems. To attain a super-critical angle at the specimen plane, the illumination must enter the back focal plane of these objectives off-axis, requiring a high numerical aperture. As such, the magnification of these objectives is generally a minimum of 60x, reducing the lateral imaging field to less than 100 μm in diameter. Sub-cellular axial resolution is therefore restricted to a tiny population of cells and statistically significant data sampling may be difficult to achieve.

To address this, we have developed a TIRF illuminator for the Mesolens, a custom giant objective lens with a 4x/0.47NA specification. The Mesolens provides an imaging field of 4.4 mm x 3.0 mm, and in combination with our new TIRF illuminator which we call MesoTIRF we have performed imaging of large cell populations with sub-micron resolution in three-dimensions. With MesoTIRF we demonstrate more than a 5-fold improvement in SBR and significantly reduced photobleaching rate compared to widefield epifluorescence illumination. We will present details of the MesoTIRF system together with current and emerging applications in cell imaging.

**Keywords:** TIRF, cell imaging, mesoscopy, optical development, high throughput, super-resolution

## 1. INTRODUCTION

Super-resolution microscopy is a many faceted niche of optical microscopy, where many intersecting sciences have cooperatively advanced the resolution achievable, elucidating detail previously only obtainable from electron micrographs, [4], [5]. Many techniques which utilize photo-switchable fluorophores, [6] or structured illumination, [7], to side step the lateral diffraction limit of the imaging objective lens may also utilize evanescent illumination to improve the axial resolution. Total Internal Reflection Fluorescence (TIRF) microscopy exploits the evanescent byproduct of a beam undergoing total internal reflection to exclusively excite fluorophores in a characteristic 100 – 300 nm depth, allowing for a much higher contrast and level of resolvable detail than that observed with a conventional widefield fluorescence microscope [8].

Single Molecule Spectroscopy and Superresolution Imaging XVI, edited by Ingo Gregor, Felix Koberling, Rainer Erdmann, Proc. of SPIE Vol. 12386, 1238604
© 2023 SPIE · 1605-7422 · doi: 10.1117/12.2649070

However, current means of achieving TIRF illumination suffer from a common drawback. The axial super-resolution and improved contrast of TIRF has been limited to a field of view of around 100 µm diameter [9], illuminating only a handful of cells, with no opportunity to examine the response or properties of the imaged cells over a statistically meaningful population without sequential imaging.

Decoupling illumination from detection allows for TIRF to be achieved with a chosen objective lens, in principle allowing for any size of lateral imaging field. By utilizing the older means of generating TIR for fluorescence imaging, a glass prism can be mounted below the sample plane of the microscope and an external illumination source can be brought to a super-critical angle at the prism face forming this plane. The balancing act now facing the TIRF illuminator is that is that faced by large field of view (FOV) microscopy: a larger imaging field comes at a forfeit in lateral resolution. While we can indeed acquire a large FOV image with a low magnification lens and super-resolution axial resolution, this may not be very useful if sub-cellular detail is lost laterally.

To address this bottleneck, we have developed a prism based TIRF illuminator for the custom giant FOV objective lens, the Mesolens, [10]. The Mesolens was designed to image full mouse embryos while retaining sub-cellular detail throughout its large imaging volume. The physical size and detailed testing of each large Mesolens component gives rise to an optical throughput 25x that of a comparable magnification lens, [10]. This enhancement in optical throughput allows for a much-improved light collection efficiency over the large FOV afforded by the low magnification. For the purposes of TIRF imaging, this manuscript will focus on the Mesolens in widefield in 2 dimensions, where the FOV is 4.4 mm x 3.0 mm, lateral resolution is 700 nm and widefield axial resolution is 7 µm. In such a physically large objective, the back focal plane is not a well-defined point as it is in commercial TIRF objectives, where illumination is focused off-axis in order to achieve a super-critical angle at the specimen plane. This fact, coupled with practicality and costing, incentivized the authors to pursue an external prism based MesoTIRF modality.

In this manuscript, we will present the optical setup of the modality, a biological characterization of its functionality as a TIRF illuminator and demonstrate its ability in cellular imaging of fine spatial detailed specimens. We will also discuss the future aims of conventional MesoTIRF imaging and further super-resolution imaging with the modality.

## 2. METHODS

### 2.1 Illuminator design

The excitation laser chosen was the tunable wavelength output of a Titanium Sapphire (Chameleon Ultra II, Coherent) pumped Optical Parametric Oscillator (Compact OPO-Vis, Coherent). When used in second harmonic generation mode, this allowed for two spectrally separate 150 mW 500 nm and 585 nm beams to be produced. These wavelengths were chosen to match the CoolLED LEDs and custom emission and dichroic filters in the Mesolens detection path. Following bench top attenuation if necessary, the beam/s were steered to the MesoTIRF illuminator.

The majority of the optical components of the MesoTIRF modality (elements L1 through M6 in Figure 1) were built onto an optical bench tower which could be moved in and out of place from the eyepiece face of the Mesolens in a fairly non-invasive manner. To install the MesoTIRF prism (Mesolens Ltd.), the existing Prior sub-micron-precision microscope stage was dropped to its minimum position, its compliant stage removed and replaced with either a glass or opaque prism stage, with the 45° edge facing towards the user. The final mirror element M6 was tilted to achieve a chosen super-critical angle at the top face of the prism, which was measured geometrically using the reflection beam from the planar exit face of the prism.

### 2.2 Specimen preparation

Cell lines used in this work were maintained in culture under conditions reported previously, [11]. Once cells grew to a high confluency in culture, a dilution was seeded onto fibronectin treated 13 mm diameter coverslips and permitted to adhere overnight in culture conditions. Following buffering and permeabilization of coverslip plated cells in solution of PBS, 2.5% FBS and 0.3% TritonX-100 (X100-100ML, Sigma Aldrich), cells were either directly labelled with the nuclear marker SYTOGreen or the F-actin stain Fluorescein Phalloidin or incubated at 4° with a primary antibody (1:250 dilution) against the focal adhesion protein paxillin. In the antibody case, following a 24hr incubation, the primary was taken off and the coverslip washed three times in PBS before replacing with an appropriate fluorescent secondary antibody excitable

at either ~500 nm or ~585 nm. Following an hour incubation at room temperature in light tight conditions and three PBS washes, the cultured and labelled coverslip was mounted underneath a larger 45 $mm^2$ coverslip with 1% agarose.

### 2.3 Biological test of evanescence

Murine fibroblast cells (3T3-L1) were labeled with both a fluorescent nuclear marker and an antibody labelling against the cell membrane focal adhesion protein paxillin. Assuming the presence of an evanescent field, the nuclear marker would be visible in widefield but with MesoTIRF the cell nucleus would be too far above the basal membrane to be excited by the evanescent wave. To image the SYTO Green stain, the camera exposure time and gain were set to 2 s and 1 X, respectively for both widefield and MesoTIRF. In widefield, the 504 nm LED power was adjusted to 25 mW to excite fluorescence from the stained nuclei without saturation. For MesoTIRF, the maximum available laser power at the specimen plane of 3.48 mW was used at a wavelength of 500 nm. To image the paxillin channel, the camera exposure time and gain were set to 2 s and 70 X, respectively for both modalities. The optical powers of the 584 nm LED (22 mW) and the 585 nm laser (3.48 mW) were adjusted to produce similar fluorescence intensities on the fly in the Mesolens' acquisition software. To estimate the number of cells, the *Surfaces* model in Imaris (Imaris 9.8, Oxford Instruments) was used for object detection of SYTO Green labeled nuclei in the widefield image.

A comparison of signal-to-background ratio (SBR) in each modality was measured via profiles in ImageJ, [12], through 3 neighbouring focal adhesions in the images from each modality. Following transfer of this data to Python, the peaks of each line profile where detected using the find_peaks() function in the SciPy library, [13], and scaled against the minimum signal intensity.

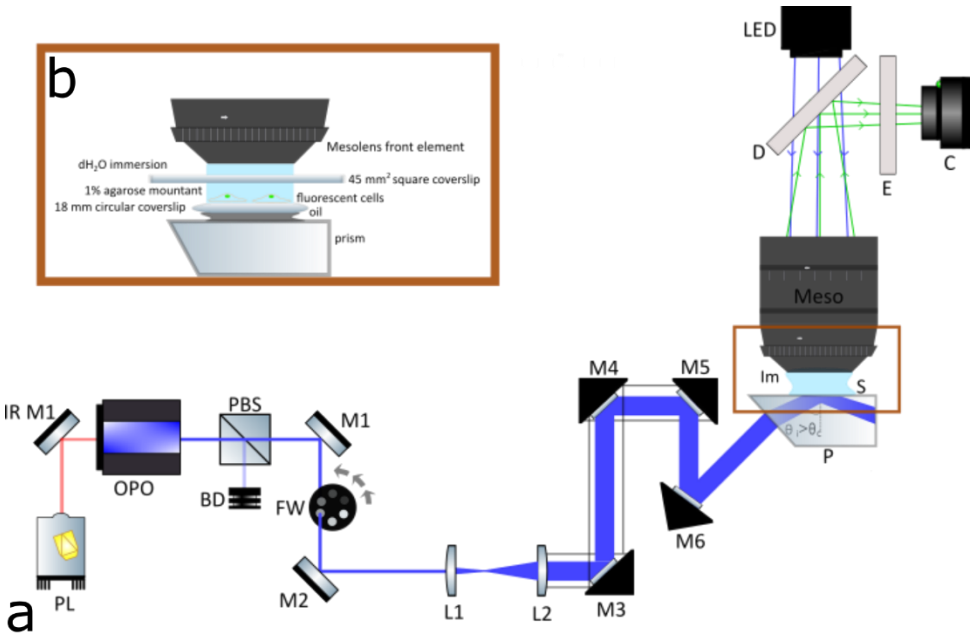


Figure 1: (a) Schematic of MesoTIRF optical path. PL: Titanium Sapphire pump laser (Ultra II, Coherent), IR M1: Infrared mirror (BB1-E03, Thorlabs), OPO: Optical Parametric Oscillator (Chameleon OPO-Vis, Coherent), PBS: polarizing beam splitter (CCMS-PBS201/M, Thorlabs), BD: beam dump, M1-6: visible broadband dielectric mirrors (Thorlabs, BB1-E01), FW: filter wheel with 5 neutral density filters (Thorlabs, FW1A), L1: 50 mm planoconvex lens (LA1131-A-ML, Thorlabs), L2: 100 mm planoconvex lens (LA1509-A-ML, Thorlabs), M3-6 mounted in right angled cage mounts (KCB1C/M, Thorlabs), P:45° borosilicate glass prism (Mesolens Ltd.), S: sample, Im: immersion fluid (distilled water), Meso: Mesolens objective element, D: dichroic filter & E: emission filter(custom from Chroma), C: chip-shifting camera sensor (VNP-29MC; Vieworks), LED: 504 nm and 584 nm LEDs from LED module (pE-4000, CoolLED).(b) illustration of specimen mounting procedure for MesoTIRF imaging

## 3. RESULTS

The biological proof of concept of the MesoTIRF modality is succinctly contained in Figure 2. Following the methods described in **2.3**, cells were imaged, analyzed and compared against the hypothesis that an evanescently illuminated specimen would not excite fluorescence in the cell nuclei. This is precisely what is observed. In Figure 2C and the digitally zoomed region of interest 2D, under similar image acquisition settings, the nuclei are not visible in the MesoTIRF channel. This is also shown quantitatively in the cyan signal in 2E. Furthermore, this figure shows another crucial characteristic of the MesoTIRF modality, namely its improvement in SBR over its widefield Mesolens counterpart. From the signals in Figure 2F, SBR improvement of 4.84 X/3.9 X/3.87 X was observed in focal adhesions 1, 2 and 3 (measured from peaks left to right). An overall improvement in image background was also determined as 4.2x in MesoTIRF compared to widefield. This reduction in background is doubly evident here, quantitatively from the intensity profile signals and visually in the images in the reduction of non-specific fluorescence and binding of the anti-paxillin antibody (magenta) to cytosolic protein. Using the specified tool, 743 cells were identified from the widefield image by analyzing the fairly uniform nuclear signal. The confirmation of our hypothesis, the measurements showing improved signal to background ratio and the fact that this TIRF-like image quality is observed hundreds and not tens of cells leads the authors to be confident in the ability of this modality.

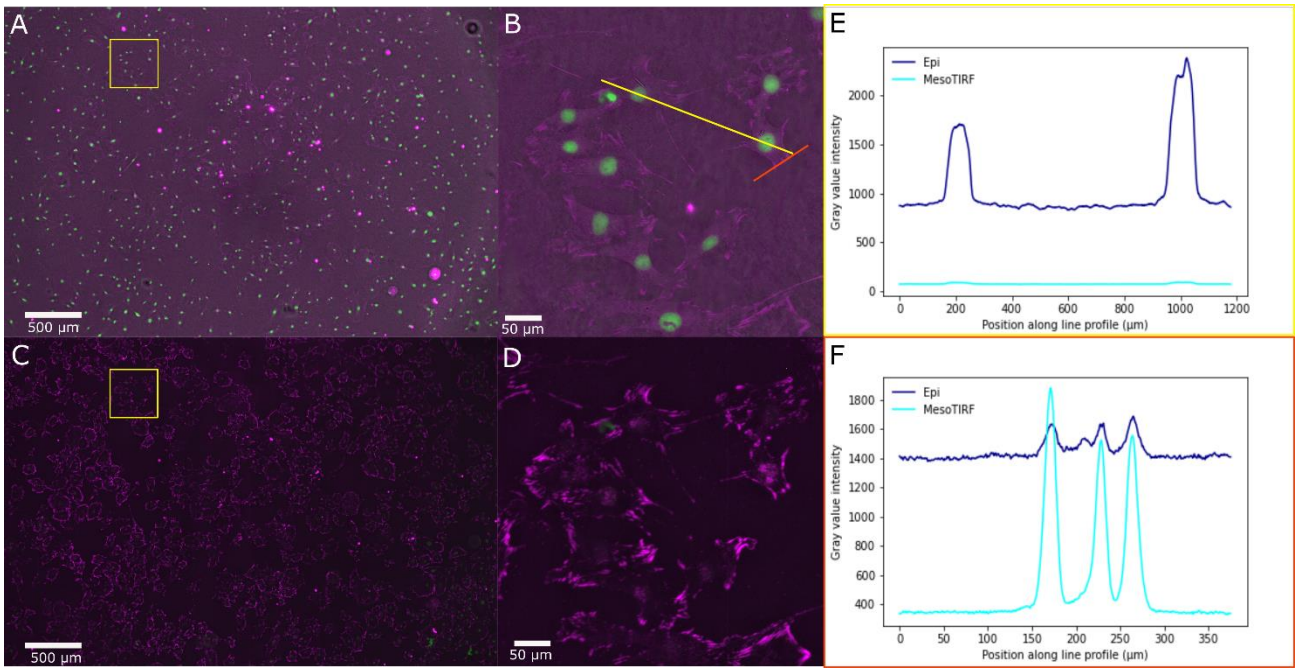


Figure 2: Validation of evanescent field production compared against widefield epi-fluorescence imaging. Fixed murine 3T3-L1 cells, nuclei labelled with SYTO9 Green and focal adhesion visualized with an anti-paxillin antibody conjugated to Alexa Fluor Plus 594. A: full Mesolens FOV under same illumination powers from 504 nm and 584 nm LEDs, channels obtained sequentially. B: digital zoom of A, illustrating two line region of interests to measure intensities of nuclei and SBR. C: MesoTIRF image obtained with 500 nm and 58 nm OPO SHG illumination. D: digital zoom of C, where same line profiles illustrated in B were also obtained. E: Raw line profile intensity through two neighbouring nuclei in widefield epi-fluorescence image (dark blue) and MesoTIRF (light blue). F: Raw line profile intensity through three neighbouring focal adhesions in both modalities.

A second fixed cell specimen was prepared with two spectrally separate fluorescent labels against two proteins which would be within the reach of an evanescent field, paxillin and F-actin, shown as a video in Figure 3. For each image channel here, a camera exposure time of 2 s and gain of 30X was used. In work, we demonstrated the uniformity of this illumination which allows for the examination of the different cell morphologies and adhesion properties at the time of fixation. The zoom in the video in Figure 3 is fully digital: the Mesolens itself is not a zoom lens. It is simply the

combination of low magnification and relatively high numerical aperture that gives rise to the high optical throughput with sub-cellular resolution.

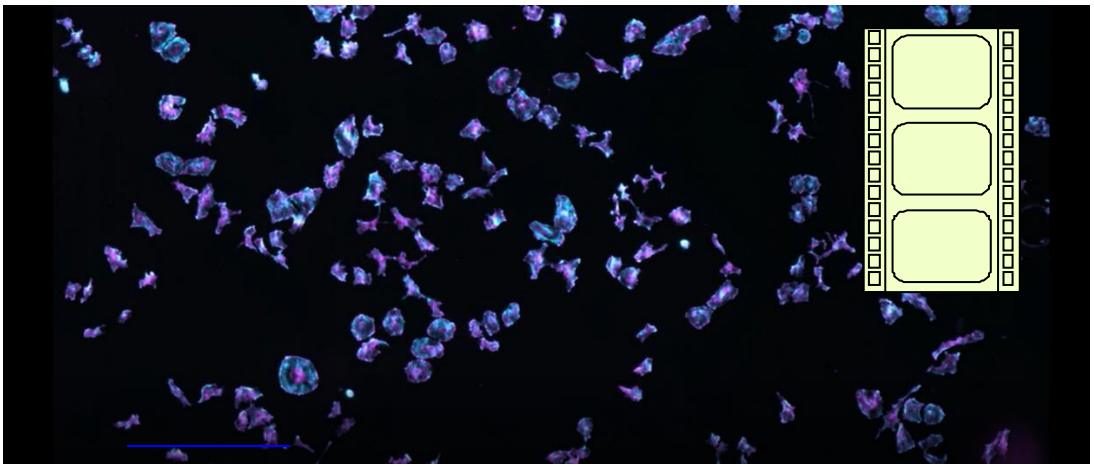

Figure 3: Fixed HeLa cells labelled with an anti-paxillin antibody conjugated to Alexa Fluor Plus 594 (magenta) and Fluorescein Phallodin which stains the actin cytoskeleton (cyan). Computational zoom from full 4.4 mm x 3.0 mm FOV of MesoTIRF image down to individually resolved focal adhesions with > 5-fold reduction in SBR when compared against widefield epi-fluorescence. http://dx.doi.org/10.1117/12.2649070.1

## 4. CONCLUSIONS

We have demonstrated the ability of the developed MesoTIRF modality for achieving high contrast imaging of fine structural detail across > 700 cells simultaneously. By designing an external prism illuminator for the Mesolens, we have been able to benefit from the 25-fold improvement in optical throughput versus a conventional objective of comparable magnification while also addressing the scale issue facing current TIRF imaging. The temporal resolution of the images obtained here was set by the sensor shifting camera, which takes 5 s to capture and register a single 4.4 mm x 3.0 mm image. At present, there are some constraints to imaging with MesoTIRF. Firstly, the temporal resolution is fixed in widefield by the camera, which necessitates examining either fixed or relatively slowly moving specimens. Secondly, there is currently not the possibility for environmental control, requiring specimens to be maintainable at room temperature in water immersion.

Looking ahead, the demonstration of MesoTIRF is encouraging for further super-resolution imaging. A common multimodal super-resolution microscopy approach is combining TIRF with Structured Illumination Microscopy (SIM). TIRF-SIM combines the nanometric axial resolution afforded by TIRF with the two-fold improvement in lateral resolution achieved by illuminating the specimen with at least 9 periodically distinct diffraction patterns. Achieving SIM with a NA of 0.47 is not a trivial endeavor and would require additional custom optics in the Mesolens light path to impose these variable patterns, or computational techniques such as blind SIM algorithms Fourier ptychography. This would however introduce the possibility of extending the resolution of the Mesolens even further into MesoTIRF-SIM.

## REFERENCES


[1] A. E. Ward, V. Kiessling, O. Pornillos, J. M. White, B. K. Ganser-Pornillos, and L. K. Tamm, “HIV-cell membrane fusion intermediates are restricted by Serincs as revealed by cryo-electron and TIRF microscopy,” *Journal of Biological Chemistry*, vol. 295, no. 45, pp. 15183–15195, Nov. 2020, doi: 10.1074/JBC.RA120.014466.

[2] M. J. Taylor, D. Perrais, and C. J. Merrifield, “A High Precision Survey of the Molecular Dynamics of Mammalian Clathrin-Mediated Endocytosis,” *PLoS Biol*, vol. 9, no. 3, p. e1000604, 2011, doi: 10.1371/JOURNAL.PBIO.1000604.

[3] A. Bella, M. Shaw, S. Ray, and M. G. Ryadnov, “Filming protein fibrillogenesis in real time,” *Sci Rep*, vol. 4, no. 1, pp. 1–6, Dec. 2014, doi: 10.1038/srep07529.
[4] R. Henriques, C. Griffiths, E. Hesper Rego, and M. M. Mhlanga, “PALM and STORM: Unlocking live-cell super-resolution,” *Biopolymers*, vol. 95, no. 5, pp. 322–331, May 2011, doi: 10.1002/bip.21586.
[5] L. Schermelleh *et al.*, “Super-resolution microscopy demystified,” *Nat Cell Biol*, vol. 21, no. 1, p. 72, Jan. 2019, doi: 10.1038/s41556-018-0251-8.
[6] I. Jayasinghe *et al.*, “True Molecular Scale Visualization of Variable Clustering Properties of Ryanodine Receptors,” *Cell Rep*, vol. 22, no. 2, pp. 557–567, Jan. 2018, doi: 10.1016/j.celrep.2017.12.045.
[7] M. G. L. Gustafsson, “Surpassing the lateral resolution limit by a factor of two using structured illumination microscopy,” *J Microsc*, vol. 198, no. 2, pp. 82–87, May 2000, doi: 10.1046/j.1365-2818.2000.00710.x.
[8] D. Axelrod, “Cell-substrate contacts illuminated by total internal reflection fluorescence,” *J Cell Biol*, vol. 89, no. 1, pp. 141–145, Apr. 1981, doi: 10.1083/jcb.89.1.141.
[9] D. A. Coucheron, Ø. I. Helle, C. I. Øie, J. C. Tinguely, and B. S. Ahluwalia, “High-Throughput Total Internal Reflection Fluorescence and Direct Stochastic Optical Reconstruction Microscopy Using a Photonic Chip,” *JoVE (Journal of Visualized Experiments)*, vol. 2019, no. 153, p. e60378, Nov. 2019, doi: 10.3791/60378.
[10] G. McConnell, J. Trägårdh, R. Amor, J. Dempster, E. Reid, and W. B. Amos, “A novel optical microscope for imaging large embryos and tissue volumes with sub-cellular resolution throughout,” *Elife*, vol. 5, p. e18659, Sep. 2016, doi: 10.7554/eLife.18659.
[11] J. K. Schniete *et al.*, “An evaluation of multi-excitation-wavelength standing-wave fluorescence microscopy (TartanSW) to improve sampling density in studies of the cell membrane and cytoskeleton,” *Sci Rep*, vol. 11, no. 1, p. 2903, Feb. 2021, doi: 10.1038/S41598-020-78282-6.
[12] C. T. Rueden *et al.*, “ImageJ2: ImageJ for the next generation of scientific image data,” *BMC Bioinformatics*, vol. 18, no. 1, p. 529, Nov. 2017, doi: 10.1186/s12859-017-1934-z.
[13] P. Virtanen *et al.*, “SciPy 1.0: fundamental algorithms for scientific computing in Python,” *Nat Methods*, vol. 17, no. 3, pp. 261–272, Mar. 2020, doi: 10.1038/s41592-019-0686-2.